JCB Article

Noninvasive two-photon imaging reveals retinyl ester storage structures in the eye

Yoshikazu Imanishi,[1] Matthew L. Batten,[1] David W. Piston,[4] Wolfgang Baehr,[5] and Krzysztof Palczewski[1,2,3]

[1]Departments of Ophthalmology, [2]Pharmacology, and [3]Chemistry, University of Washington, Seattle, WA 98195
[4]Department of Molecular Physiology and Biophysics, Vanderbilt University Medical Center, Nashville, TN 37232
[5]Departments of Ophthalmology, Biology, and Neurobiology and Anatomy, University of Utah Health Science Center, Salt Lake City, UT 84112

Visual sensation in vertebrates is triggered when light strikes retinal photoreceptor cells causing photoisomerization of the rhodopsin chromophore 11-cis-retinal to all-trans-retinal. The regeneration of pre-illumination conditions of the photoreceptor cells requires formation of 11-cis-retinal in the adjacent retinal pigment epithelium (RPE). Using the intrinsic fluorescence of all-trans-retinyl esters, noninvasive two-photon microscopy revealed previously uncharacterized structures (6.9 ± 1.1 μm in length and 0.8 ± 0.2 μm in diameter) distinct from other cellular organelles, termed the retinyl ester storage particles (RESTs), or retinosomes. These structures form autonomous all-trans-retinyl ester-rich intracellular compartments distinct from other organelles and colocalize with adipose differentiation-related protein. As demonstrated by in vivo experiments using wild-type mice, the RESTs participate in 11-cis-retinal formation. RESTs accumulate in *Rpe65*$^{-/-}$ mice incapable of carrying out the enzymatic isomerization, and correspondingly, are absent in the eyes of *Lrat*$^{-/-}$ mice deficient in retinyl ester synthesis. These results indicate that RESTs located close to the RPE plasma membrane are essential components in 11-cis-retinal production.

Introduction

Metabolic transformations of retinoids within the retinal photoreceptor and retinal pigment epithelium (RPE) are responsible for the production of the chromophore essential for vision, 11-cis-retinal (McBee et al., 2001). Within the RPE, all-trans-retinol (vitamin A), a product of photoisomerized and reduced 11-cis-retinal, is esterified with fatty acids in a reaction catalyzed by lecithin:retinol acyltransferase (LRAT; Fig. 1; Saari et al., 1993). LRAT was identified on the molecular level as a 25-kD protein (Ruiz et al., 1999) that is expressed in several tissues, including liver and the RPE (for review see McBee et al., 2000). All-trans-retinyl esters are intermediate compounds in a pathway ("retinoid cycle") that recycles 11-cis-retinal, the chromophore of the visual pigments of rod and cone photoreceptors (for review see Bok, 1985; McBee et al., 2001). All-trans-retinyl esters have been suggested to be the substrate for a putative isomerohydrolase in the RPE (Rando, 1991) and for a retinyl ester hydrolase that produces all-trans-retinol, a substrate for the putative isomerase (for review see McBee et al., 2000). Regardless of the enzymatic pathway, 11-cis-retinol is produced, oxidized to 11-cis-retinal, and exported to the photoreceptors where it recombines with opsins to form 11-cis-retinylidene-opsins (rhodopsin, and cone pigments; Fig. 1; for review see Filipek et al., 2003).

Defects in the retinoid cycle may lead to blinding disorders, such as retinitis pigmentosa or macular degeneration (Rattner et al., 1999; Dryja, 2000; Baehr et al., 2003). Among these, the inherited early onset dystrophies are collectively called Leber congenital amaurosis (LCA). LCA is a group of genetically heterogeneous diseases that involves, among others, mutations in LRAT and RPE-specific 65-kD protein (RPE65) genes (Gu et al., 1997; Marlhens et al., 1997; Morimura et al., 1998; Perrault et al., 1999; Thompson et al., 2001). Animal models of these specific LCA were generated (Redmond et al., 1998; Batten et al., 2003) to address functional consequences of the targeted gene disruption on

The online version of this article includes supplemental material.

Address correspondence to Krzysztof Palczewski, Dept. of Ophthalmology, University of Washington, 1959 NE Pacific St., Box 356485, Seattle, WA 98195-6485. Tel.: (206) 543-9074. Fax: (206) 221-6784. email: palczews@u.washington.edu

Key words: retinoid cycle; photoreceptor cells; two-photon microscopy; retinal pigment epithelial cells; rhodopsin

Abbreviations used in this paper: 3-D, three-dimensional; ADRP, adipose differentiation-related protein; CRALBP, cellular retinaldehyde-binding protein; LRAT, lecithin:retinol acyltransferase; REST, retinyl ester storage particle; ROS, rod outer segment; RPE, retinal pigment epithelium; RPE65, an RPE-specific 65-kD protein.

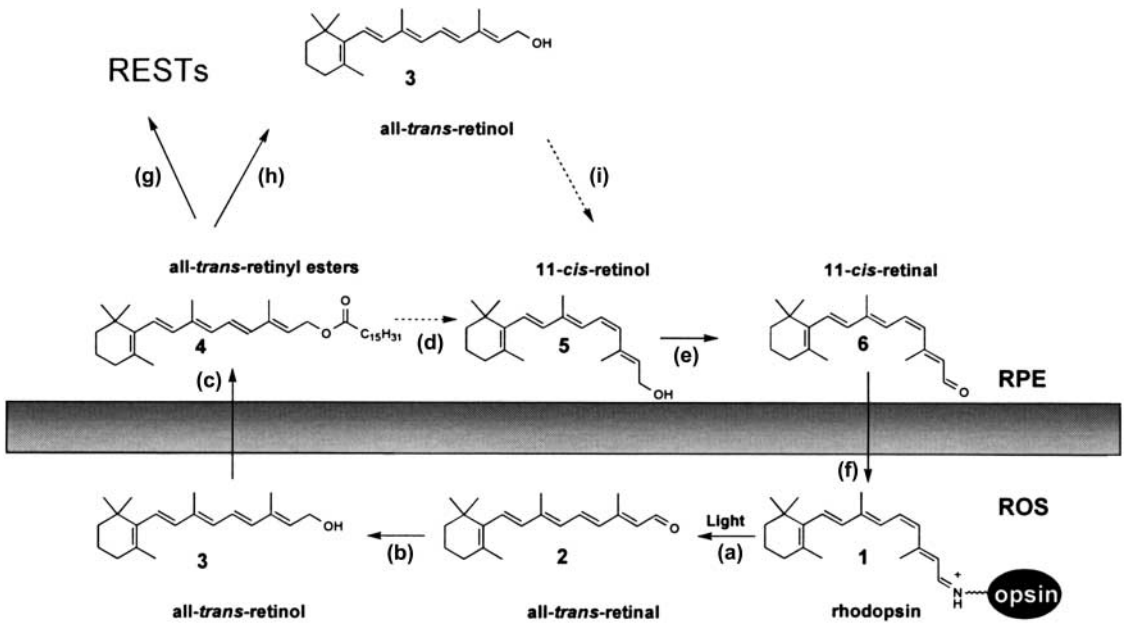

Figure 1. **Chemistry of retinoid cycle reactions in the vertebrate retina.** Retinoid cycle reactions were reviewed previously (McBee et al., 2001). In the rod outer segment (ROS), light causes the isomerization (reaction a) of the rhodopsin chromophore, 11-cis-retinylidene (1), to all-trans-retinylidene. All-trans-retinal (2) is hydrolyzed and then reduced (reaction b) in the reaction catalyzed by all-trans-retinal–specific RDH(s). All-trans-retinol (3) diffuses to the RPE, where it is esterified by LRAT (reaction c) to all-trans-retinyl esters (4). Retinyl esters form RESTs (g). All-trans-retinyl esters can be hydrolyzed by a yet-unidentified retinyl ester hydrolase (reaction h) generating all-trans-retinol. All-trans-retinol (3) or its esters (4) is isomerized to 11-cis-retinol (5) in a reaction that involves an RPE-abundant protein, termed RPE65 (incompletely defined reactions d or i). 11-cis-retinol is then oxidized by 11-cis-RDH and other dehydrogenases to 11-cis-retinal (6) (reaction e) to complete the cycle (modified version from Jang et al., 2000). 11-cis-retinal diffuses back to the ROS, where it recombines with opsin to reform rhodopsin.

the retinoid metabolism. Recently, somatic gene therapy and pharmacological intervention were successful in restoration of vision in the dog and mouse animal models of LCA, respectively, with the nonfunctional RPE65 gene (Van Hooser et al., 2000, 2002; Acland et al., 2001).

Although several retinoid metabolites are generated during regeneration of 11-cis-retinal, only retinol and retinyl esters show a weak intrinsic fluorescence (excitation λ at $\sim$320 nm; Sears and Kaplan, 1989; Garwin and Saari, 2000; Kuksa et al., 2003; Zipfel et al., 2003). Simultaneous absorption of two photons and excitation of intrinsic fluorophores, in conjunction with laser scanning fluorescence microscopy (Denk et al., 1990; Bennett et al., 1996), has been exploited to generate three-dimensional (3-D) temporal and spectral-resolved images of cells, tissues, or organs (Euler et al., 2002; Wang et al., 2003). Here, infrared two-photon microscopy was used to monitor changes in the distribution of vitamin A and its metabolites in the intact mouse eye without mechanical disruption of the essential close contacts between the photoreceptor and the RPE, photobleaching of rhodopsin, or photodamage to the tissue. The retinyl ester storage structures increased in the RPE of wild-type mice exposed to light or in an age-dependent manner in light- and dark-adapted *Rpe65*$^{-/-}$ mice incapable of carrying out the enzymatic isomerization, and they were absent in the eyes of *Lrat*$^{-/-}$ mice deficient in vitamin A. Thus, two-photon microscopy revealed changes in the retinyl ester pool in normal and pathological states in vivo, without disruption of the fragile RPE–retina interface.

Results

Identification of retinyl ester storage particles in wild-type RPE

Two-photon microscopy, with excitation at $\lambda = 730$ nm directly through the sclera of the dissected mouse eye, revealed a clear image of fluorescent compartments $\sim$50 μm (390–545-nm emission; Fig. 2 A, red pseudocolor) and within $\sim$1–40 μm (560–700-nm emission) from the surface of the sclera (Fig. 2 A, green pseudocolor). Taking advantage of the layered structure of the eye (Kolb et al., 2001), the two fluorescent compartments were localized within the RPE (red) and the sclera (green). Localization of these compartments was deduced based on morphological criteria, such as appropriate distances verified by histological sectioning (unpublished data), differences in the appearance of nuclei in each layer (Fig. 2 A, right column), and on the appearance of the capillaries in the choroid. RPE fluorescence in the unstained eyecup displayed unique elongated structures perpendicular to the cell layer with a length of 6.9 ± 1.1 μm, a diameter of 0.8 ± 0.2 μm, and frequency of 36.2 ± 2.2 per double-nuclei cells ($n = 200$; Fig. 2 B, a). 3-D projections of these fluorescent structures present in the RPE showed particular localization and remarkable symmetry (Video 1, available at http://www.jcb.org/cgi/content/full/jcb.200311079/DC1). Antibodies against RPE-dominant transmembrane 11-cis-retinol dehydrogenase (Fig. 2 B, b), membrane-associated RPE65 (Fig. 2 B, c), and soluble cellular retinaldehyde-binding protein (CRALBP; Fig. 2 B, d) confirmed the intracellular position of the autofluorescent structures. 3-D pro-

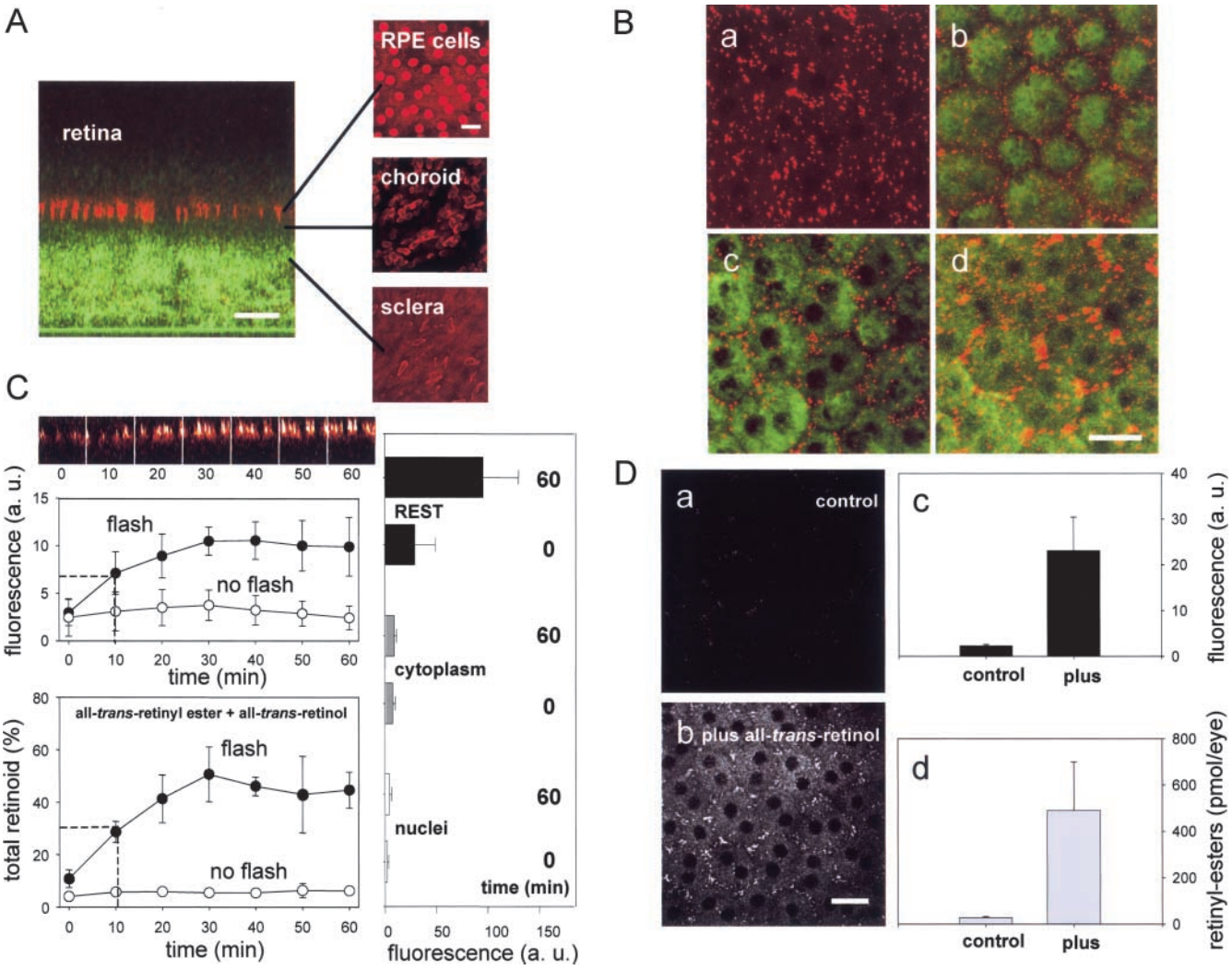

Figure 2. **Identification of autofluorescent structures in the wild-type mouse RPE.** (A) Fluorescence emission from the isolated intact mouse eye. Two fluorescence emissions (390–545 nm in red pseudocolor and 560–700 nm in green pseudocolor) were observed when excited by a 730-nm mode-locked Ti:Sapphire laser. The right column shows tangential optical sections of the eyecup stained by Hoechst 33342. Note the circular structures in the RPE panel. 4-wk-old mice were used in all experiments. (B) Arrangement of RESTs in the RPE. A projection of the highly fluorescent structures in the RPE in the eyecup that are aligned perpendicularly to the RPE cell layer and that we termed RESTs, or retinosomes (a). The immunolocalization of 11-cis-retinol dehydrogenase (b, green), RPE65 (c, green) and CRALBP (d) in comparison to the autofluorescent RESTs (red). (C) Flash-dependent changes in fluorescence and all-trans-retinol/all-trans-retinyl esters in the RPE cell layer in isolated eyes. Top: a row of images showing the optical sections of the retina, radial to the ocular tissue. The RPE fluorescence (a.u., arbitrary unit) was quantified in a time-dependent manner. The numbers refer to minutes after flash. Middle and bottom graphs show the quantified fluorescence from retinoids and retinoid analysis by HPLC (all-trans-retinol and all-trans-retinyl esters; mean ± SD, $n = 3$), respectively. Dashed lines indicate the half-time formation of RESTs and the increase in all-trans-retinol and all-trans-retinyl esters. On the right, the light-dependent changes in the fluorescent signal in different subcellular compartments. (D) Supplementation of all-trans-retinol to the RPE cell layer in the eyecup. (a) The single RPE layer before addition of all-trans-retinol. (b) The RPE after exposure to all-trans-retinol for 2 min. (c) Changes in averaged fluorescence intensity under the same conditions as in a and b (mean ± SD, $n = 30$ for three independent measurements). (d) Amount of retinyl ester in eyecup samples of c as quantified by normal phase HPLC (mean ± SD, $n = 3$). Bars, 20 μm.

jections of these fluorescent structures (red) and anti-11-cis-retinol dehydrogenase immunostaining (green) in the RPE demonstrated that they did not colocalize (Video 2). Similarly, 3-D projections of these structures (red) and anti-RPE65 immunostaining (green) in the RPE showed that they are present in nonoverlapping cellular compartments (Video 3).

Bleaching of rhodopsin in the intact rod-dominant mouse eye led to time-dependent increase in fluorescence within the RPE layer with the half-time $\tau_{1/2} = 10$ min ($n = 3$), without significant changes within the rod outer segments (ROSs; Fig. 2 C, top two left panels). The change paralleled a light-dependent increase in the formation of all-trans-retinol and all-trans-retinyl esters ($\tau_{1/2} = 10$ min; $n = 3$) in the RPE as determined by normal phase HPLC (Fig. 2 C, bottom left; Van Hooser et al., 2002), suggesting these structures contain retinoids. The fluorescence signal localized specifically to these subcellular structures, which we termed retinyl ester storage particles (RESTs), or retinosomes. The fluorescence signal increase coincided

with formation of all-trans-retinol/all-trans-retinyl esters (unpublished data). The results for a 60-min incubation in the dark are shown in Fig. 2 C (right). These data are consistent with earlier observations that the visual cycle does not proceed to the 11-cis-retinoid production in the dissected eyes and eyecups (Palczewski et al., 1999), and that under physiological temperature- and oxygen/carbonated-control conditions the reaction mostly proceeds to all-trans-retinyl ester formation (~65%; unpublished data). When the eyecups were incubated with a soluble complex of vitamin A ((2-hydroxypropyl)-β-cyclodextrin·all-trans-retinol), significant increases in fluorescence and all-trans-retinyl ester formation were observed in these structures (Fig. 2 D, b). The increases in the fluorescence intensity coincided with increases of the retinyl ester content (Fig. 2 D, c and d), strengthening the argument that these structures contain the fluorescent retinyl esters. No tissue damage was observed after two-photon excitation, as determined by the analysis of histological sections.

Colocalization of RESTs with adipose differentiation-related protein in wild-type RPE

Fluorescent RESTs are not a part of Golgi (Fig. 3 a), mitochondria (Fig. 3 b), a majority of lysosomes (Fig. 3 c), the plasma membrane (Fig. 3 d), or the ER (Fig. 3 e). RESTs also did not colocalize with autofluorescent A2E, a component of lipofuscin, an age-related by-product of ROS phagocytosis by the RPE (Liu et al., 2000; unpublished data). NADH and NADPH were poorly excited at 730 nm and were not observed in our experiments, as demonstrated by the lack of mitochondrial fluorescence (see also Kuksa et al., 2003). The RESTs did not colocalize with peroxisomes, as visualized by immunofluorescence techniques with catalase, a marker of these organelles (unpublished data). However, using immunocytochemistry, we found that adipose differentiation-related protein (ADRP) colocalizes with the RESTs (Fig. 3 f). ADRP was shown previously to localize at the vicinity of the plasma membrane involved in the formation and stabilization of lipid droplets (Gao and Serrero, 1999; Targett-Adams et al., 2003).

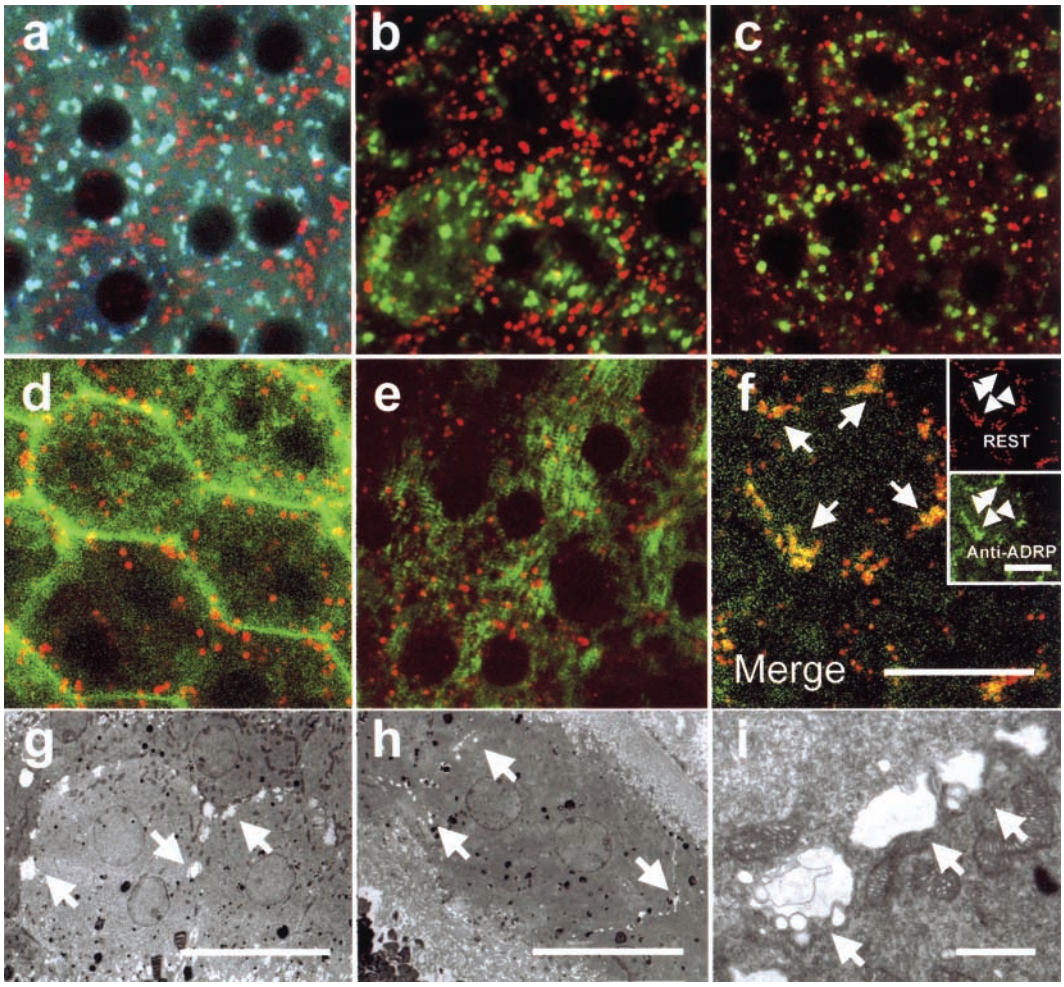

Figure 3. **Organelle-autonomous localization of RESTs in the wild-type RPE, REST colocalization with ADRP, and the REST ultrastructure.** (a–e) Localization of RESTs (red) and other RPE subcellular organelles in the mouse eyecup. (a) Golgi apparatus (light blue); b, mitochondria (green); c, acidic organelles including lysosomes (green); d, plasma membranes (green); e, ER (green); f, colocalization of ADRP and RESTs (yellow) in fixed mouse eyecup. Inset: top, REST localization (red); bottom, immunolocalization of ADRP (green). (g–i) Subcellular organization of the RPE by EM. (g) Mouse eyes were fixed 30 min after bleaching of rhodopsin to facilitate all-trans-retinyl ester accumulation in the RPE. Lipid droplet-like structures (~1 μm in the diameter) are often observed close to the cell boundary (arrows). (h) Dark-adapted mouse eye. Lipid droplet-like structures are smaller (arrows) than those observed in g. (i) Higher magnification of the image shown in g. RESTs are indicated by arrows. An electron-dense coating and membranes surrounded the lipid-like structure. Bars: 20 μm (a–f), 10 μm (g and h), 1 μm (i).

Tangential sections of the RPE, analyzed by EM, showed that most of the mouse RPE contained two nuclei (Fig. 3, g and h), as observed in rats (Owaribe et al., 1988). Moreover, vacuole-like structures with translucent inclusions were often present close to the boundary of the cells (Fig. 3, g and h). After flash stimulation of rhodopsin (Fig. 3 g), the vacuole-like structures were more inflated compared with those kept in the dark (Fig. 3 h). The diameters of the structures were ~1 μm after flash stimulation (Fig. 3 i). Electron-dense vesicles observed throughout the cell were membrane inclusions (ingested ROS) or peroxisomes. The location, size, and frequency of the vacuole-like structures corresponded with RESTs observed by two-photon microscopy, suggesting that RESTs may incorporate retinyl esters, thereby increasing their volume.

RESTs in normal and mutant RPE

If RESTs participate in production of 11-cis-retinal, no light-dependent changes in two-photon excited autofluorescence should be observed in the RPE of mice lacking a functional RPE65 gene, which is essential for chromophore regeneration (Redmond et al., 1998). Although the wild-type RPE increased their fluorescence intensity (arbitrary unit) from 0.56 ± 0.28 to 1.52 ± 0.56 after an intense 10-ms flash that bleached ~60% of the pigment (Fig. 4 A, a, b, and g), these changes were not observed in the RPE of *Rpe65*$^{-/-}$ mice (Fig. 4 A, c, d, and g). Consistently, the amounts of all-trans-retinyl esters increased from 71.4 ± 3.3 to 274.2 ± 32.4 pmol for wild-type mice, whereas for the eyes of *Rpe65*$^{-/-}$ mice the amount was 207.6 ± 19.5 pmol for pre-flash conditions and comparable to 192.3 ± 6.6 pmol post-flash (Fig. 4 A, g).

LRAT could be the enzyme essential for trapping retinoids from bleached photoreceptors and for removing them from the circulation (McBee et al., 2001). Hence, *Lrat*$^{-/-}$ mice were generated and analyzed (Batten et al., 2003). Total retinoid analyses revealed that the eyes of *Lrat*$^{-/-}$ mice contained residual amounts of retinoids (~8.3 pmol/eye in 4-wk-old mice) and no functional rhodopsin (Batten et al., 2003). For

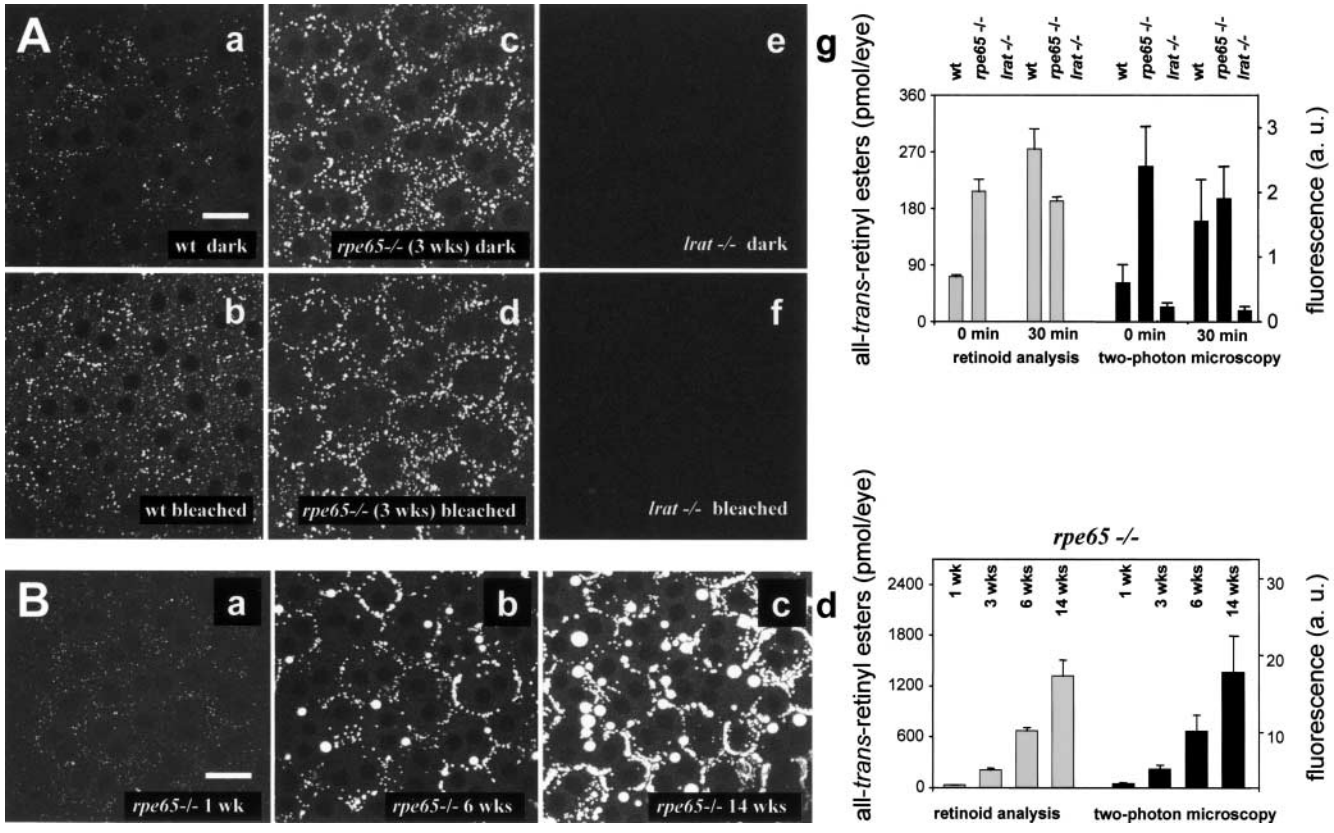

Figure 4. **RESTs in the RPE of *Rpe65*$^{-/-}$ and *Lrat*$^{-/-}$ mice.** (A) The deficiency of light-induced changes of RESTs in the *Rpe65*$^{-/-}$ and *Lrat*$^{-/-}$ mouse eyes. (a and b) RPE autofluorescence in 6-wk-old wild-type mouse before flash stimulation and 30 min after bleaching of rhodopsin, respectively. (c and d) RPE autofluorescence in 3-wk-old *Rpe65*$^{-/-}$ mouse before flash and after flash stimulation, respectively. (e and f) The RPE cell layer of *Lrat*$^{-/-}$ mouse before flash and after flash stimulation, respectively. (g) Quantitative determination of all-trans-retinyl esters in a mouse eye by HPLC. Gray bars represent the total amount of all-trans-retinyl ester per eye (left y-axis) under each genetic background at the indicated time after flash stimulation of rhodopsin. Error bars represent mean ± SD (n = 30 from three mouse eyes). Black bars on the right show the intensity of RPE autofluorescence (right y-axis) from mice of different genetic backgrounds. (B) Age-dependent accumulation of all-trans-retinyl esters into RESTs in the RPE of *Rpe65*$^{-/-}$ mice. At the age of 1 wk (a), the formation of RESTs is observed as a slight accumulation of all-trans-retinyl esters (a). At the age of 6 wk (b), strong accumulation of all-trans-retinyl esters in RESTs and formation of lipid droplets of all-trans-retinyl esters are observed. 14-wk-old mice (c) show additional fluorophore accumulation in RESTs and form bigger lipid droplets compared with those in 6-wk-old animals. (d) Quantified fluorescence and the level of all-trans-retinyl esters in the eyes of *Rpe65*$^{-/-}$ mice at the given age. Gray bars indicate the quantified all-trans-retinyl esters in the eyes of *Rpe65*$^{-/-}$ mice of different age. Black bars indicate the quantified fluorescence. The measurements were performed as described in A (g). Bars, 20 μm.

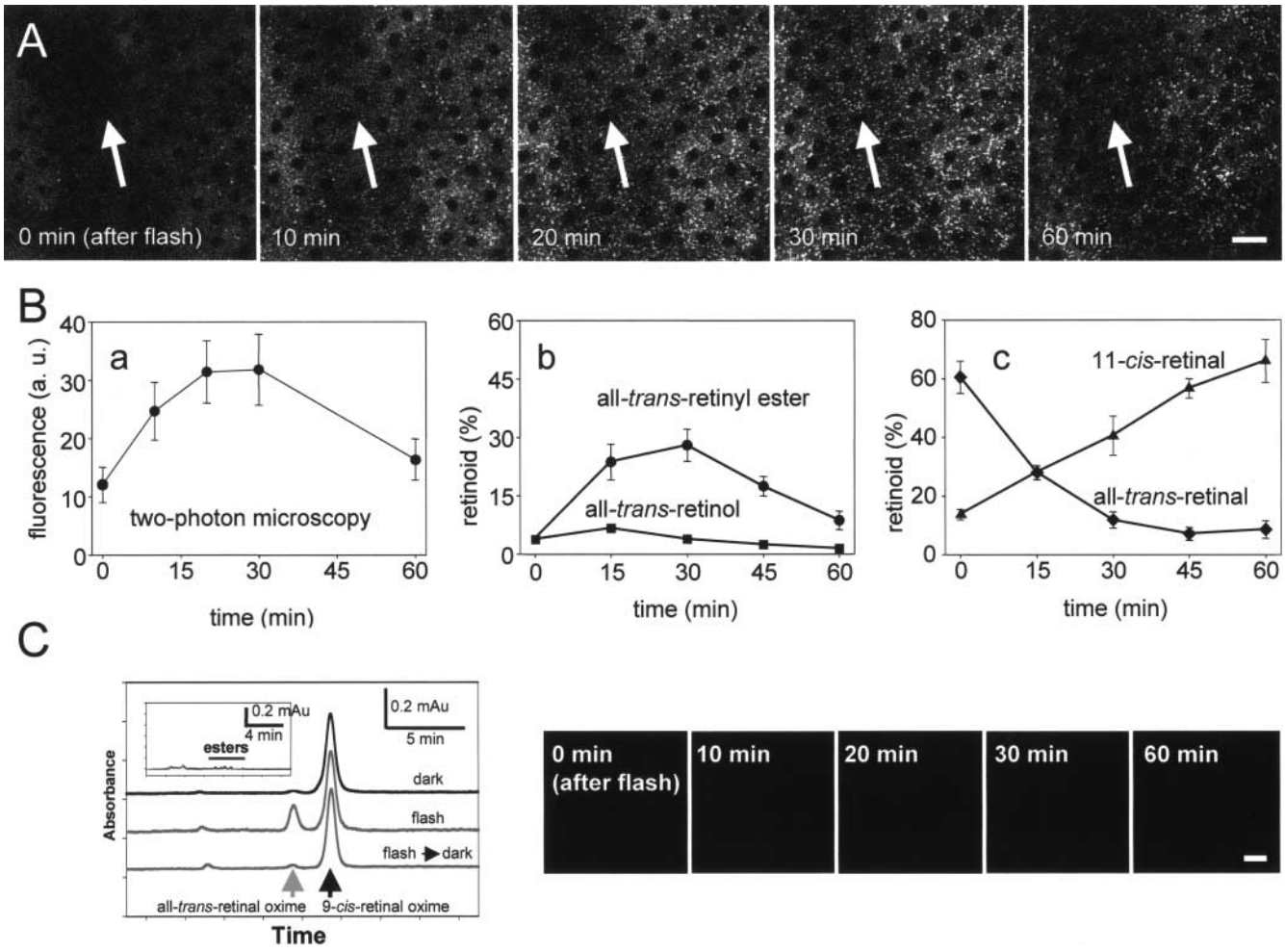

Figure 5. **RESTs participate in 11-cis-retinal production in mice.** (A) Two-photon vitamin A imaging in the anesthetized wild-type mouse. Images were collected at the peripheral area of the RPE. Intense flashes were given to the eye and images were collected at the given times after flash. The area below a blood vessel shows weaker fluorescence (arrows). Bar, 20 μm. (B) Comparison of fluorescent intensity and the amount of retinoids. (a) Time course of transient changes in fluorescent intensity. Fluorescence was measured for randomly chosen areas. (b and c) Each retinoid species (percentage of total retinoid) was quantified by normal phase HPLC. (b) Changes in the transient amount of all-trans-retinyl esters were observed in parallel to the fluorescent intensity quantified in panel a. All-trans-retinol increased slightly 15 min after flash stimulation and then decreased. (c) Increase of 11-cis-retinal and decay of all-trans-retinal level after flash stimulation. The level of individual retinoid is expressed as a percentage of the total retinoids (sum of retinals, retinols, and retinyl esters). (C) Lack of REST formation in the RPE of *Lrat*$^{-/-}$ mice gavaged with 9-cis-retinal. *Lrat*$^{-/-}$ mice were gavaged as described previously (Van Hooser et al., 2000) with 2.5 mg of 9-cis-retinal. After 36 h in the dark, mice were exposed to intense flash that bleached ~30% of the visual pigment. One group was analyzed for the retinoid content 1 min after flashes, and the other group was analyzed 3 h after flash followed by dark adaptation (top absorption profile, dark-adapted; middle absorption profile, 1 min after flash; bottom absorption profile, 3 h after flash). Under the same conditions, mice were also analyzed by two-photon microscopy to image the RPE after bleach. Note the lack of ester formation (inset) and REST formation (right panels). Bar, 20 μm.

comparison, ~500 pmol retinoid/eye was present in the wild-type or *Lrat*$^{+/-}$ littermates, mostly in opsin-bound 11-cis-retinylidene form. Because only trace amounts of all-trans-retinol and retinyl esters were present in the RPE of *Lrat*$^{-/-}$ mice (Fig. 4 A, g; Batten et al., 2003), the RESTs are not formed (Fig. 4 A, e and f). No light-dependent changes in the retinoid levels as assayed by fluorescence or HPLC were observed in the eyes of *Lrat*$^{-/-}$ mice (Fig. 4 A, e–g).

In the RPE of *Rpe65*$^{-/-}$ mice, age-dependent increase in formation of lipid droplet-like structures filled with a translucent lipid-like substance was attributed to all-trans-retinyl ester accumulation (Van Hooser et al., 2002). Therefore, we investigated REST formation as a function of age in the RPE of *Rpe65*$^{-/-}$ mice. Here, a systematic increase of retinoids was observed with increasing age in the RPE of these mice (Fig. 4 B). The increase in RPE fluorescence intensity paralleled the increase in the all-trans-retinyl ester accumulation (Fig. 4 B, d) and formation of a spherical body, morphologically distinct from normal RESTs, within the RPE. These results provide the first direct evidence that the "oil-droplets" (Redmond et al., 1998) are formed, at least in part, from all-trans-retinyl esters.

RESTs and flow of retinoids in the retinoid cycle

To observe directly whether RESTs participate in the flow of retinoids, we extended our analyses to live mice. We acquired fluorescence images at the periphery of the retina di-

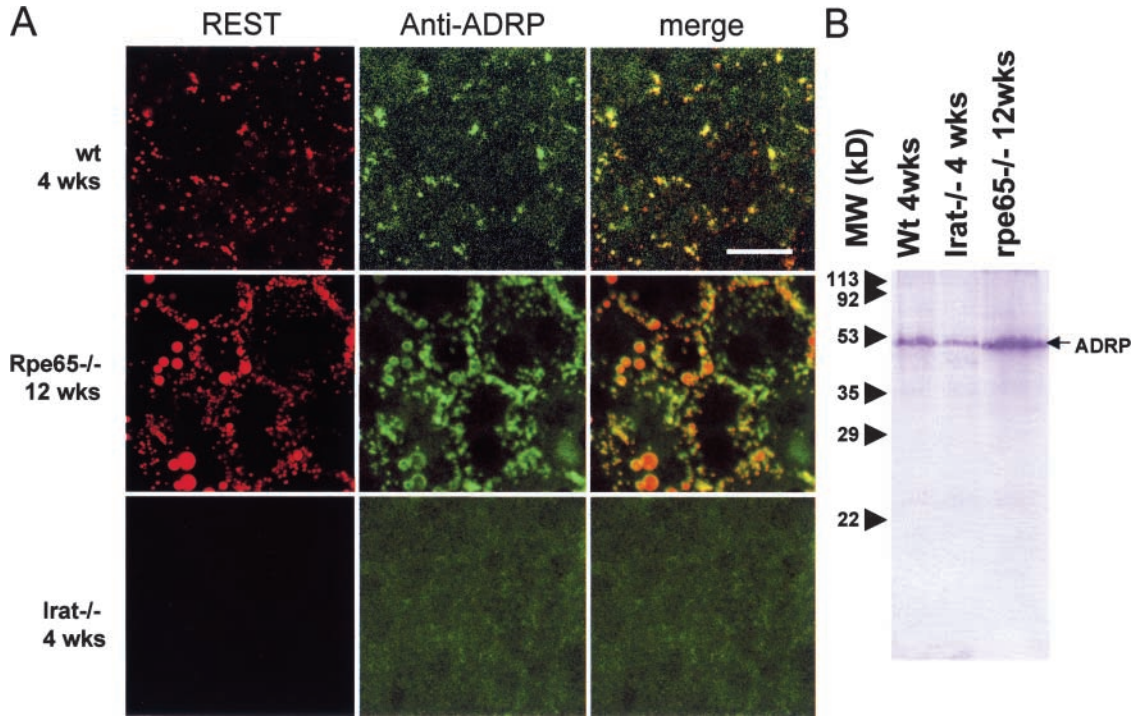

Figure 6. **Colocalization of ADRP and RESTs in the wild-type and mutant RPE.** (A) Immunofluorescent localization of ADRP (green) covisualized with RESTs (red). Left column shows the localization of RESTs imaged by two-photon microscopy. Middle column shows the localization of ADRP. Right column shows the colocalization of ADRP (green) and RESTs (red). The top row is allocated for 4-wk-old wild-type mouse, middle row for 12-wk-old *Rpe65*$^{-/-}$ mouse, and bottom row for 4-wk-old *Lrat*$^{-/-}$ mouse. Colocalization of RESTs and ADRP were observed as yellow color in the wild-type and *Rpe65*$^{-/-}$ mouse. Localization of ADRP in *Lrat*$^{-/-}$ was diffusive and RESTs were not observed. Bar, 20 μm. (B) Relative abundance of ADRP protein in the eyes of mice with different genetic backgrounds. Eyecup extracts were prepared from half of the eye and were separated by SDS-PAGE, blotted onto membrane, and detected by anti-ADRP antibodies. The method of immunoblots was as described previously (Haeseleer et al., 2002), with the exception that a goat anti–guinea pig AP-conjugated antibody (Jackson ImmunoResearch Laboratories) was used as the secondary antibody.

rectly through the sclera, using thoroughly dark-adapted and anesthetized mice (Fig. 5 A). After a light flash, the change in the fluorescence intensity of RESTs paralleled the formation of all-trans-retinyl esters in the RPE of those mice (Fig. 5 B). The retinyl ester pool peaked at 30 min (Fig. 5 B, b) and the regeneration of 11-cis-retinal is nearly completed within 60 min (Saari et al., 1998), corresponding to formation of 11-cis-retinal and disappearance of all-trans-retinal (Fig. 5 B, c). On light stimulation, the number of RESTs appeared to be similar as in the RPE of the dark-adapted mice, but their intensity increased significantly.

To test whether RESTs are essential for the isomerization process, we gavaged *Lrat*$^{-/-}$ mice with 9-cis-retinal, as described previously for *Rpe65*$^{-/-}$ mice (Van Hooser et al., 2002). 9-cis-retinal recombined with opsin, forming isorhodopsin, as demonstrated by the analysis of retinoids in the eye, UV-Vis spectroscopy of the detergent extract from the eye, and isolation of isorhodopsin by immunoaffinity chromatography (unpublished data). After bleach, 9-cis-retinal bound to opsin was converted to all-trans-retinal. Without formation of retinyl ester, and hence RESTs, all-trans-retinal/all-trans-retinol were quickly lost from the eye (Fig. 5 C). Accordingly, no formation of 11-cis-retinal (with different chromatographic and spectral properties from 9-cis-retinal) was observed. These results demonstrate that RESTs participate in retinoid storage and restoration of the chromophore after photobleaching.

RESTs and ADRP in mutant animals

Because ADRP colocalized with the RESTs (Fig. 3 f), we investigated whether its expression and localization is altered in genetically engineered mice that have enhanced accumulation of all-trans-retinyl esters or lack them entirely. The overaccumulation of all-trans-retinyl esters in the RPE of *Rpe65*$^{-/-}$ mice coincided with accumulation of ADRP in the RESTs as observed in the eyes of *Rpe65*$^{-/-}$ mice. In contrast, ADRP was present throughout the RPE cytoplasm of *Lrat*$^{-/-}$ mice lacking retinyl esters (Fig. 6, A and B). In the RPE cells of *Lrat*$^{-/-}$ mice, ADRP was expressed at lower levels (Fig. 6 B), which suggests that ADRP is a protein component of the RESTs.

Discussion

Our aim was to use native and genetically modified mice in conjunction with microscopy, HPLC, and immunocytochemistry to understand mechanisms governing the retinoid cycle and visual transduction. Spectrally sensitive noninvasive two-photon microscopy in conjunction with genetically engineered mice lacking key components of the retinoid cycle was used to identify a novel structure in the RPE involved in the production of the visual chromophore, 11-cis-retinal. Two-photon microscopy permitted deep tissue penetration of infrared excitation light in anesthetized mice to monitor regeneration processes of rhodopsin with-

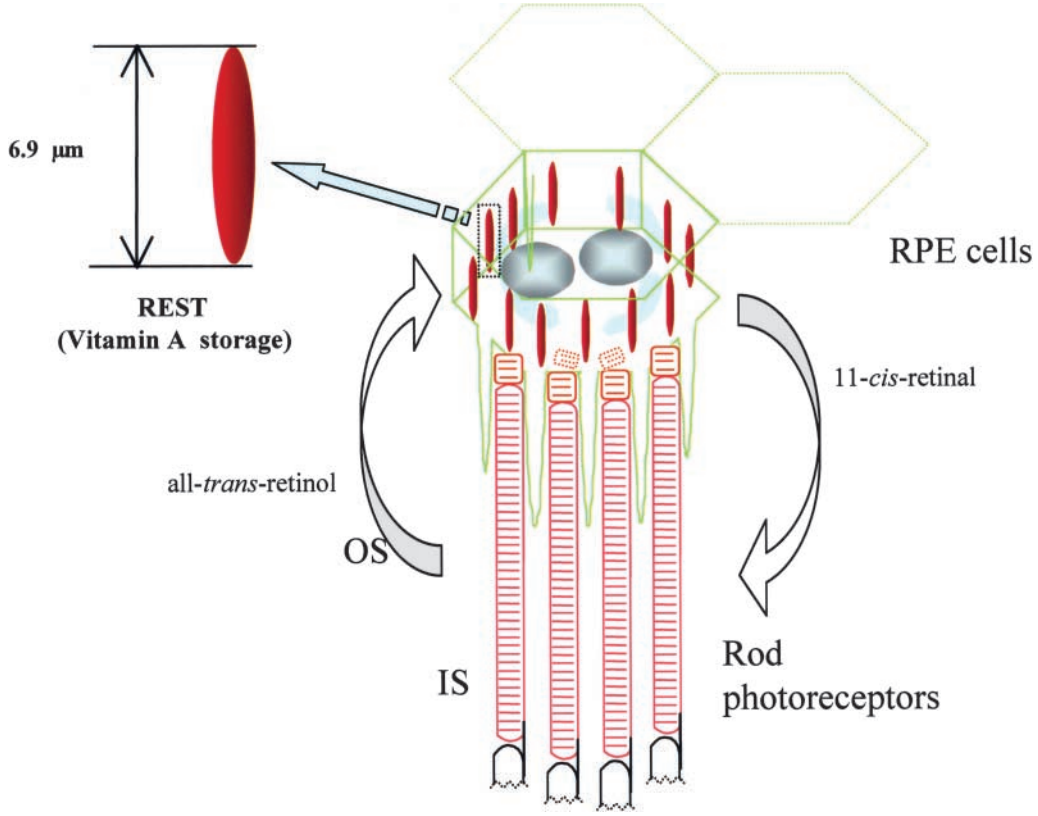

Figure 7. **RESTs in the RPE.** The RPE (hexagons) interdigitate with ROSs. Large curved arrows symbolize the flow of retinoids from and to the rod outer segments (OS). RESTs are depicted as elongated red ovals ~6.9 μm in length.

out introducing external fluorophores. Our results revealed the existence of novel structures, RESTs (or retinosomes), that are critical to the formation of 11-cis-retinal.

In wild-type mice, all-trans-retinol exchanges rapidly between the blood and the RPE (Qtaishat et al., 2003). RESTs appear to be essential structures for retaining esterified vitamin A in the eye to support its utilization in formation of the chromophore for visual pigments. RESTs are also essential for trapping all-trans-retinol generated in photoreceptors, which must diffuse across the ECM separating ROSs and the RPE. Subcellular localization of these structures allows efficient trapping of all-trans-retinol from both the choroidal circulation and from photoreceptors after photoisomerization of rhodopsin's chromophore. This process is stalled in the RPE of *Rpe65*$^{-/-}$ mice (Redmond et al., 1998; Qtaishat et al., 2003) that overaccumulate all-trans-retinyl esters in aberrantly large RESTs (Fig. 4).

The flow of soluble retinoids in either free or protein-bound form is governed by the gradient generated by the conversion of 11-cis- and all-trans-retinol to insoluble all-trans-retinyl esters in the RPE and the conversion of 11-cis-retinal to 11-cis-retinylidene-opsin in rod photoreceptor cells (McBee et al., 2001). Hence, compartmentalization plays an essential role in driving energetically unfavorable chemical reactions through mass action (McBee et al., 2001). The all-trans-retinyl esters constitute a storage intermediate in the isomerization pathway from all-trans- to 11-cis-isomers (Rando, 1996). The isomerization proceeds through a reaction that involves an unidentified enzyme-retinol intermediate, or a specific subpopulation of all-trans-retinyl esters with properties that are distinct from the bulk of all-trans-retinyl esters (Stecher et al., 1999). All-trans-retinyl esters present in the RESTs and formed in situ on the internal membranes where LRAT resides may form two subpopulations, from which only one is used for the isomerization process directly.

Several molecular components involved in the 11-cis-retinal formation have been identified through biochemical and genetic approaches. RPE65 is thought to be involved in the delivery of all-trans-retinyl esters to the isomerization machinery by the virtue of specific binding of these esters (Gollapalli et al., 2003; Mata et al., 2004). Our analyses add a cell biological view for the formation of retinyl esters during the retinoid cycle. All-trans-retinol likely diffuses first to the ER, where the major fraction is converted to retinyl esters by the ER-localized LRAT. Our in vivo analysis demonstrates that the retinyl esters are next delivered to and stored in RESTs. Blocking the redistribution of all-trans-retinyl esters from RESTs resulted in aberrant accumulation of all-trans-retinyl esters in RESTs as observed in the RPE of *Rpe65*$^{-/-}$ mice. In photoreceptors of *Lrat*$^{-/-}$ mice regenerated with 9-cis-retinal, photoisomerization of isorhodopsin (9-cis-retinylidene-opsin) produced all-trans-retinoids, which could not be converted to 11-cis-retinal, hence formation of rhodopsin (11-cis-retinylidene-opsin) was not observed. Free all-trans-retinol could be quickly lost to the circulation, whereas all-trans-retinyl esters are essential in the retention of retinoids in the eye. This observa-

tion does not discard the possibility that all-trans-retinol is used directly by a putative isomerase, simply because all-trans-retinyl esters could be the starting substrate for the RPE65–hydrolase–isomerase complex indispensable in the production of 11-cis-retinol.

On average, between 20 and 40 ROSs project toward one RPE cell (for review see McBee et al., 2001). For efficient transfer of retinoid between the RPE and the photoreceptor cells, the retinoid-processing enzymes should be widely distributed throughout the cell as observed in this and previous reports (McBee et al., 2001; Haeseleer et al., 2002; Batten et al., 2003). Once the retinoids are esterified, they are trapped into RESTs (Fig. 7), which are composed of all-trans-retinyl esters and at least one additional protein component, ADRP. The formation of self-associating complexes of all-trans-retinyl esters (Li et al., 1996) could facilitate REST formation. Clustering of all-trans-retinyl esters may prevent diffusion of retinoids through the retina, and may circumvent overproduction of all-trans-retinoic acid, an agent known to cause cell differentiation and proliferation (Mangelsdorf et al., 1995), thus lowering overall toxicity. However, the symmetric nature of these structures and their intracellular distribution suggest that perhaps additional proteins are also involved. Interestingly, Liu et al. (2003) provided evidence that the lipid droplets in CHO K2 cells are metabolic organelles involved in membrane traffic, and that they contained ADRP as a major protein component of these structures termed adiposomes. It is tempting to speculate that ADRP could be an essential component of the lipid structures throughout the body.

Prior reports of myeloid bodies in the RPE have demonstrated that they vary in size during light adaptation (Tabor and Fisher, 1983; Abran and Dickson, 1992a,b; Dickson and Morrison, 1993; Cai and Dickson, 1994), suggesting possible involvement in the retinoid cycle. However, the appearance and location of the REST is different from the myeloid bodies, and the relationship between these two structures is unclear. Robison and Kuwabara (1977) observed accumulation of lipid inclusion droplets along the basal and lateral cell boundaries after injection of the substantial dose of all-trans-retinyl esters. In our experiments, the subcellular localization of the RESTs, a minor component of the RPE, and appearance of these structures differ from those previous observations. Most EM analyses were performed on radial sections of the eye, and hence it was difficult to provide quantitative results for the thin structures perpendicularly aligned to the RPE cell layer. A combination of EM and application of two-photon microscopy to study visual processes using the infrared laser for the excitation of the fluorophores opens a new way to detect and study the subcellular structures.

In summary, in this work we have used the power of noninvasive, spectrally sensitive two-photon microscopy in conjunction with genetically engineered mice lacking key components of the retinoid cycle to define a novel structure in the RPE, the RESTs (Fig. 7). Two-photon microscopy has unsurpassed potential to advance our understanding of normal physiological processes and to provide new insights into the pathology of many other eye diseases using suitable mouse models.

Materials and methods

Animals

The University of Washington and University of Utah Animal Care Committees approved all of the procedures that used animal experiments. Animals were maintained in complete darkness, and all of the manipulations with animals, dissected eyes, or retinoids were performed under dim red light using a No. 1 Safelight filter (transmittance >560 nm; Kodak). The Balb/c mice were used as a wild type throughout the experiments. *Rpe65*$^{-/-}$ mice were obtained from Dr. M. Redmond (National Eye Institute, National Institutes of Health, Bethesda, MD). *Lrat*$^{-/-}$ mice were generated as recently described (Batten et al., 2003). Albino lines of *Rpe65*$^{-/-}$ and *Lrat*$^{-/-}$ mice were maintained in a mixed background of 129Sv, C57Bl/6, and Balb/c. *Rpe65*$^{-/-}$ mice were genotyped as described previously (Redmond et al., 1998). Mice were anesthetized by i.p. injection using 15 μl/g body weight of 6 mg/ml ketamine and 0.44 mg/ml xylazine diluted with 10 mM phosphate buffer, pH 7.2, containing 100 mM NaCl. The gavage experiments were performed on *Lrat* mice as described for *Rpe65* mice in Van Hooser et al. (2002).

Multiphoton vitamin A imaging

Two-photon excitation microscopy was performed using a confocal microscope (LSM 510 MP-NLO; Carl Zeiss MicroImaging, Inc.) with LSM510 software v3.0. Briefly, 76-MHz, 100-fs pulses of 730-nm light from a mode-locked Ti:Sapphire laser (Mira-900; Coherent) were focused on the sample by a Plan-Neofluar 40×/1.3 NA objective lens for ex vivo experiments and a Planapochromat 20×/0.75 NA lens for in vivo experiments (Carl Zeiss MicroImaging, Inc.). The intensity of the laser was measured at the back aperture of the objective lens and kept at ~3 mW for ex vivo analysis and ~5 mW for in vivo analysis. For 3-D imaging of RESTs in Fig. 1 B, the average power of the laser was kept at ~10 mW. Autofluorescence from the sample (390–545 nm) was collected by the objective, separated from the excitation light by a dichroic mirror, filtered to remove scattered excitation light, and directed to a photomultiplier tube detector. The objective lens was heated to 37°C by an air stream incubator. A temperature-controlled microscopic stage was installed on the microscope to maintain the reaction at 37°C. Fluorescent intensities reflected in pixel values were calculated by off-line analysis of the collected raw images (SCION image; Scion Co.). Fluorescent intensity was measured for the tangential sections of the RPE, and was averaged per pixel for randomly chosen areas (mean ± SD; $n = 30$ from three eyes) enclosing 100 × 100 pixels (~30 × 30 μm^2 for Fig. 1 B and C and Fig. 3; 36 × 36 μm^2 for Fig. 4). For separation of the cytoplasmic, nucleic, and REST responses (Fig. 1 B, right), fluorescent intensities were averaged for randomly chosen areas of 25 pixels (~2 μm^2; $n = 180$ for three independent eyes). In Fig. 1 D, the RPE was exposed to 1.4 mM all-trans-retinol caged with 100 mM (2-hydroxypropyl)-β-cyclodextrin for 2 min, and was washed briefly with Ames medium (Sigma-Aldrich) for 3 min.

For ex vivo imaging, immediately after eye removal, mouse eyes or eyecups were located at the center of a glass-bottomed 35-mm dish and perfused with oxygenized (95% O_2, 5% CO_2) Ames medium at 37°C. For in vivo observation, an anesthetized mouse was laid on the temperature-controlled microscopic stage (at 37°C), and the right side of the eye was located on the microscopic cover glass (44-mm-diam, 0.16-mm thickness; Carl Zeiss MicroImaging, Inc.). In this way, the retina was imaged at the periphery by the laser penetrating through the sclera while the emission fluorescence was collected coming back to the microscopic objective lens. In case of a slight movement of the eye, the same area of the retina was traced using unique texture of the RPE cell layer formed by the randomly arranged single- and dual-nucleated RPE. In most experiments, thoroughly dark-adapted mice were exposed to an intense 10-ms flash that bleached ~60% of the pigment.

Analysis of retinoids

Retinoids were stored in *N,N*-dimethylformamide under argon at −80°C, and the concentrations were determined spectrophotometrically (Garwin and Saari, 2000). All retinoids were purified by normal phase HPLC (Ultrasphere-Si, 4.6 mm × 250 mm; Beckman Coulter) with 10% ethyl acetate/90% hexane at a flow rate of 1.4 ml/min (Van Hooser et al., 2000).

Immunocytochemistry and fluorescent visualization of subcellular organelles

Eyecups were prepared by removing anterior segments and neural retinas from the isolated mouse eyes, and the exposed RPE was fixed with 4% PFA for 15 min at 37°C. Immunofluorescence detection of antigens by anti-RPE65 antibody (a gift of M. Redmond, National Eye Institute), anti-

CRALBP antibody (a gift of J.C. Saari, University of Washington, Seattle, WA), anti-ADRP (Progen), and anti-11-cis-retinol dehydrogenase (Haeseleer et al., 2002) was performed as described previously (Haeseleer et al., 2002). Samples were incubated with the primary antibody for 1 h and for 30 min with the secondary antibody conjugated with Cy3 (Jackson ImmunoResearch Laboratories).

A number of fluorescent dyes (Molecular Probes, Inc.) were applied to the live RPE in the eyecup. Golgi apparatus was visualized by introducing 50 μM BODIPY® FL C_5-ceramide. Two emission ranges were collected (500–530 nm for green pseudocolor and 560–700 nm for blue pseudocolor) from the fluorophore that had two emission peaks (515 nm and ~620 nm) by excitation at 488 nm. Mitochondria were visualized by 200 nM MitoTracker® Orange CMTMRos, and emissions from 560 to 700 nm were collected by excitation at 543 nm. Acidic organelles including lysosomes were visualized by 200 nM LysoTracker® Green DND-26, and the emission range from 500 to 550 nm was collected by excitation at 488 nm. For visualization of the plasma membrane, 1 mM FM 4-64 was applied to the RPE and emission was collected at ~650 nm (λ_{ex} = 543 nm). $DiOC_6$ dye was applied at 5 μg/ml to visualize the ER, and the emission was collected from 500 to 550 nm excited at 488 nm. A2E (green) was visualized by collecting emission from 565 to 615 nm by excitation at 488 nm. Fluorescent signals were covisualized with RESTs using a laser scanning microscope (LSM510; Carl Zeiss MicroImaging, Inc.) under appropriate filter configuration.

Image processing

For figure preparation, Adobe Photoshop® 6.0 was used for adjustments of brightness and for color balance. 3-D reconstructed projections shown in Fig. 1 B and in the supplemental videos were generated using LSM510 software v3.0 (Carl Zeiss MicroImaging, Inc.).

Transmission EM

Dark-adapted mice controls or dark-adapted mice exposed to an intense flash (10-ms duration) that bleached ~60% of the pigment were used for TEM. Photobleached mice were allowed to recover for 30 min to allow formation of retinyl esters. Mouse eyecups were primarily fixed by immersion in 2.5% glutaraldehyde and 1.6% PFA in 0.08 M Pipes, pH 7.4, containing 2% sucrose initially at RT for ~1 h, and then at 4°C for the remainder of 24 h (Van Hooser et al., 2002). The eyecups were then washed with 0.13 M sodium phosphate, pH 7.35, and secondarily fixed with 1% OsO_4 in 0.1 M sodium phosphate, pH 7.35, for 1 h at RT. The eyecups were dehydrated through a methanol series and transitioned to the epoxy-embedding medium with propylene oxide. The eyecups were embedded for sectioning in Eponate 812. Ultrathin sections (60–70 nm) were stained with aqueous saturated uranium acetate and Reynold's formula lead citrate before survey and micrography with an electron microscope (model CM10; Philips).

Online supplemental material

Video 1 shows retinyl ester storage particles in the RPE cells. Three-dimensional projections of retinyl ester storage particles in the RPE cells. Video 2 shows covisualization of retinyl ester storage particles and 11-cis-retinol dehydrogenase. Three-dimensional projections of retinyl ester storage particles (red) and 11-cis-retinol dehydrogenase (green) in the RPE cells. Video 3 shows covisualization of retinyl ester storage particles and RPE65. Three-dimensional projections of retinyl ester storage particles (red) and RPE65 (green) in the RPE cells.

We would like to thank Drs V. Gerke, R. Rodieck, A. Polans, and A. Moise for insightful comments on the manuscript; Dr. M. Redmond for providing *Rpe65*$^{-/-}$ mice and anti-RPE65 antibody; Dr. J.C. Saari for anti-CRALBP antibody; and D. Possin for the EM analysis.

This research was supported by National Institutes of Health grants EY09339, EY13385, EY08123 (to W. Baehr), and DK53434 (to D.W. Piston); National Science Foundation grant DBI9871063 (to D.W. Piston); a grant from Research to Prevent Blindness, Inc. (RPB) to the Departments of Ophthalmology at the University of Washington and the University of Utah; the Stargardt and Retinal Eye Disease Fund; a grant from the Macular Vision Research Foundation (to W. Baehr); a Foundation for Fighting Blindness Center grant to the University of Utah; and a grant from the E.K. Bishop Foundation (to K. Palczewski). K. Palczewski and W. Baehr are RPB Senior Investigators.

Submitted: 17 November 2003
Accepted: 29 December 2003

References

Abran, D., and D.H. Dickson. 1992a. Biogenesis of myeloid bodies in regenerating newt (*Notophthalmus viridescens*) retinal pigment epithelium. *Cell Tissue Res.* 268:531–538.

Abran, D., and D.H. Dickson. 1992b. Phospholipid composition of myeloid bodies from chick retinal pigment epithelium. *Exp. Eye Res.* 54:737–745.

Acland, G.M., G.D. Aguirre, J. Ray, Q. Zhang, T.S. Aleman, A.V. Cideciyan, S.E. Pearce-Kelling, V. Anand, Y. Zeng, A.M. Maguire, et al. 2001. Gene therapy restores vision in a canine model of childhood blindness. *Nat. Genet.* 28: 92–95.

Baehr, W., S.M. Wu, A.C. Bird, and K. Palczewski. 2003. The retinoid cycle and retina disease. *Vision Res.* 43:2957–2958.

Batten, M.L., Y. Imanishi, T. Maeda, D. Tu, A.R. Moise, D. Bronson, D. Possin, R.N. Van Gelder, W. Baehr, and K. Palczewski. 2003. Lecithin:retinol acyltransferase (LRAT) is essential for retention of retinyl esters in the eye and in the liver. *J. Biol. Chem.*10.1074/jbc.M312410200.

Bennett, B.D., T.L. Jetton, G. Ying, M.A. Magnuson, and D.W. Piston. 1996. Quantitative subcellular imaging of glucose metabolism within intact pancreatic islets. *J. Biol. Chem.* 271:3647–3651.

Bok, D. 1985. Retinal photoreceptor-pigment epithelium interactions. Friedenwald lecture. *Invest. Ophthalmol. Vis. Sci.* 26:1659–1694.

Cai, F., and D.H. Dickson. 1994. Diurnal change and prolonged dark effect on myeloid bodies in the retinal pigment epithelium of the leopard frog. *Curr. Eye Res.* 13:611–617.

Denk, W., J.H. Strickler, and W.W. Webb. 1990. Two-photon laser scanning fluorescence microscopy. *Science.* 248:73–76.

Dickson, D.H., and C. Morrison. 1993. Diurnal variation in myeloid bodies of the chick retinal pigment epithelium. *Curr. Eye Res.* 12:37–43.

Dryja, T.P. 2000. Molecular genetics of Oguchi disease, fundus albipunctatus, and other forms of stationary night blindness: LVII Edward Jackson Memorial Lecture. *Am. J. Ophthalmol.* 130:547–563.

Euler, T., P.B. Detwiler, and W. Denk. 2002. Directionally selective calcium signals in dendrites of starburst amacrine cells. *Nature.* 418:845–852.

Filipek, S., R.E. Stenkamp, D.C. Teller, and K. Palczewski. 2003. G protein-coupled receptor rhodopsin: a prospectus. *Annu. Rev. Physiol.* 65:851–879.

Gao, J., and G. Serrero. 1999. Adipose differentiation related protein (ADRP) expressed in transfected COS-7 cells selectively stimulates long chain fatty acid uptake. *J. Biol. Chem.* 274:16825–16830.

Garwin, G.G., and J.C. Saari. 2000. High-performance liquid chromatography analysis of visual cycle retinoids. *Methods Enzymol.* 316:313–324.

Gollapalli, D.R., P. Maiti, and R.R. Rando. 2003. RPE65 operates in the vertebrate visual cycle by stereospecifically binding all-*trans*-retinyl esters. *Biochemistry.* 42:11824–11830.

Gu, S.M., D.A. Thompson, C.R. Srikumari, B. Lorenz, U. Finckh, A. Nicoletti, K.R. Murthy, M. Rathmann, G. Kumaramanickavel, M.J. Denton, and A. Gal. 1997. Mutations in RPE65 cause autosomal recessive childhood-onset severe retinal dystrophy. *Nat. Genet.* 17:194–197.

Haeseleer, F., G.F. Jang, Y. Imanishi, C.A. Driessen, M. Matsumura, P.S. Nelson, and K. Palczewski. 2002. Dual-substrate specificity short chain retinol dehydrogenases from the vertebrate retina. *J. Biol. Chem.* 277:45537–45546.

Jang, G.F., J.K. McBee, A.M. Alekseev, F. Haeseleer, and K. Palczewski. 2000. Stereoisomeric specificity of the retinoid cycle in the vertebrate retina. *J. Biol. Chem.* 275:28128–28138.

Kolb, H., R. Nelson, P. Ahnelt, and N. Cuenca. 2001. Cellular organization of the vertebrate retina. *Prog. Brain Res.* 131:3–26.

Kuksa, V., Y. Imanishi, M. Batten, K. Palczewski, and A.R. Moise. 2003. Retinoid cycle in the vertebrate retina: experimental approaches and mechanisms of isomerization. *Vision Res.* 43:2959–2981.

Li, C.Y., C.L. Zimmerman, and T.S. Wiedmann. 1996. Solubilization of retinoids by bile salt/phospholipid aggregates. *Pharm. Res.* 13:907–913.

Liu, J., Y. Itagaki, S. Ben-Shabat, K. Nakanishi, and J.R. Sparrow. 2000. The biosynthesis of A2E, a fluorophore of aging retina, involves the formation of the precursor, A2-PE, in the photoreceptor outer segment membrane. *J. Biol. Chem.* 275:29354–29360.

Liu, P., Y. Ying, Y. Zhao, D.I. Mundy, M. Zhu, and R.G. Anderson. 2003. CHO K2 cell lipid droplets appear to be metabolic organelles involved in membrane traffic. *J. Biol. Chem.*10.1074/jbc.M311945200.

Mangelsdorf, D.J., C. Thummel, M. Beato, P. Herrlich, G. Schutz, K. Umesono, B. Blumberg, P. Kastner, M. Mark, P. Chambon, et al. 1995. The nuclear receptor superfamily: the second decade. *Cell.* 83:835–839.

Marlhens, F., C. Bareil, J.M. Griffoin, E. Zrenner, P. Amalric, C. Eliaou, S.Y. Liu,

E. Harris, T.M. Redmond, B. Arnaud, et al. 1997. Mutations in RPE65 cause Leber's congenital amaurosis. *Nat. Genet.* 17:139–141.

Mata, N.L., W.N. Moghrabi, J.S. Lee, T.V. Bui, R.A. Radu, J. Horwitz, and G.H. Travis. 2004. Rpe65 is a retinyl ester binding protein that presents insoluble substrate to the isomerase in retinal pigment epithelial cells. *J. Biol. Chem*. 279:635–643. First published on October 7, 2003; 10.1074/jbc. M310042200.

McBee, J.K., V. Kuksa, R. Alvarez, A.R. de Lera, O. Prezhdo, F. Haeseleer, I. Sokal, and K. Palczewski. 2000. Isomerization of *all-trans*-retinol to cis-retinols in bovine retinal pigment epithelial cells: dependence on the specificity of retinoid-binding proteins. *Biochemistry.* 39:11370–11380.

McBee, J.K., K. Palczewski, W. Baehr, and D.R. Pepperberg. 2001. Confronting complexity: the interlink of phototransduction and retinoid metabolism in the vertebrate retina. *Prog. Retin. Eye Res.* 20:469–529.

Morimura, H., G.A. Fishman, S.A. Grover, A.B. Fulton, E.L. Berson, and T.P. Dryja. 1998. Mutations in the RPE65 gene in patients with autosomal recessive retinitis pigmentosa or leber congenital amaurosis. *Proc. Natl. Acad. Sci. USA.* 95:3088–3093.

Owaribe, K., J. Kartenbeck, E. Rungger-Brandle, and W.W. Franke. 1988. Cytoskeletons of retinal pigment epithelial cells: interspecies differences of expression patterns indicate independence of cell function from the specific complement of cytoskeletal proteins. *Cell Tissue Res.* 254:301–315.

Palczewski, K., J.P. Van Hooser, G.G. Garwin, J. Chen, G.I. Liou, and J.C. Saari. 1999. Kinetics of visual pigment regeneration in excised mouse eyes and in mice with a targeted disruption of the gene encoding interphotoreceptor retinoid-binding protein or arrestin. *Biochemistry.* 38:12012–12019.

Perrault, I., J.M. Rozet, S. Gerber, I. Ghazi, C. Leowski, D. Ducroq, E. Souied, J.L. Dufier, A. Munnich, and J. Kaplan. 1999. Leber congenital amaurosis. *Mol. Genet. Metab.* 68:200–208.

Qtaishat, N.M., T.M. Redmond, and D.R. Pepperberg. 2003. Acute radiolabeling of retinoids in eye tissues of normal and *rpe65*-deficient mice. *Invest. Ophthalmol. Vis. Sci.* 44:1435–1446.

Rando, R.R. 1991. Membrane phospholipids as an energy source in the operation of the visual cycle. *Biochemistry.* 30:595–602.

Rando, R.R. 1996. Polyenes and vision. *Chem. Biol.* 3:255–262.

Rattner, A., H. Sun, and J. Nathans. 1999. Molecular genetics of human retinal disease. *Annu. Rev. Genet.* 33:89–131.

Redmond, T.M., S. Yu, E. Lee, D. Bok, D. Hamasaki, N. Chen, P. Goletz, J.X. Ma, R.K. Crouch, and K. Pfeifer. 1998. *Rpe65* is necessary for production of 11-*cis*-vitamin A in the retinal visual cycle. *Nat. Genet.* 20:344–351.

Robison, W.G., Jr., and T. Kuwabara. 1977. Vitamin A storage and peroxisomes in retinal pigment epithelium and liver. *Invest. Ophthalmol. Vis. Sci.* 16: 1110–1117.

Ruiz, A., A. Winston, Y.H. Lim, B.A. Gilbert, R.R. Rando, and D. Bok. 1999. Molecular and biochemical characterization of lecithin retinol acyltransferase. *J. Biol. Chem.* 274:3834–3841.

Saari, J.C., D.L. Bredberg, and D.F. Farrell. 1993. Retinol esterification in bovine retinal pigment epithelium: reversibility of lecithin:retinol acyltransferase. *Biochem. J.* 291:697–700.

Saari, J.C., G.G. Garwin, J.P. Van Hooser, and K. Palczewski. 1998. Reduction of all-*trans*-retinal limits regeneration of visual pigment in mice. *Vision Res.* 38: 1325–1333.

Sears, R.C., and M.W. Kaplan. 1989. Axial diffusion of retinol in isolated frog rod outer segments following substantial bleaches of visual pigment. *Vision Res.* 29:1485–1492.

Stecher, H., M.H. Gelb, J.C. Saari, and K. Palczewski. 1999. Preferential release of 11-*cis*-retinol from retinal pigment epithelial cells in the presence of cellular retinaldehyde-binding protein. *J. Biol. Chem.* 274:8577–8585.

Tabor, G.A., and S.K. Fisher. 1983. Myeloid bodies in the mammalian retinal pigment epithelium. *Invest. Ophthalmol. Vis. Sci.* 24:388–391.

Targett-Adams, P., D. Chambers, S. Gledhill, R.G. Hope, J.F. Coy, A. Girod, and J. McLauchlan. 2003. Live cell analysis and targeting of the lipid droplet-binding adipocyte differentiation-related protein. *J. Biol. Chem.* 278:15998–16007.

Thompson, D.A., Y. Li, C.L. McHenry, T.J. Carlson, X. Ding, P.A. Sieving, E. Apfelstedt-Sylla, and A. Gal. 2001. Mutations in the gene encoding lecithin retinol acyltransferase are associated with early-onset severe retinal dystrophy. *Nat. Genet.* 28:123–124.

Van Hooser, J.P., T.S. Aleman, Y.G. He, A.V. Cideciyan, V. Kuksa, S.J. Pittler, E.M. Stone, S.G. Jacobson, and K. Palczewski. 2000. Rapid restoration of visual pigment and function with oral retinoid in a mouse model of childhood blindness. *Proc. Natl. Acad. Sci. USA.* 97:8623–8628.

Van Hooser, J.P., Y. Liang, T. Maeda, V. Kuksa, G.F. Jang, Y.G. He, F. Rieke, H.K. Fong, P.B. Detwiler, and K. Palczewski. 2002. Recovery of visual functions in a mouse model of Leber congenital amaurosis. *J. Biol. Chem.* 277:19173–19182.

Wang, J.W., A.M. Wong, J. Flores, L.B. Vosshall, and R. Axel. 2003. Two-photon calcium imaging reveals an odor-evoked map of activity in the fly brain. *Cell.* 112:271–282.

Zipfel, W.R., R.M. Williams, R. Christie, A.Y. Nikitin, B.T. Hyman, and W.W. Webb. 2003. Live tissue intrinsic emission microscopy using multiphoton-excited native fluorescence and second harmonic generation. *Proc. Natl. Acad. Sci. USA.* 100:7075–7080.